2024 IEEE/RSJ International Conference on Intelligent Robots and Systems (IROS)
October 14-18, 2024. Abu Dhabi, UAE

Potential Field-Based Online Path Planning for Robust Cable Routing

Andrea Monguzzi[1], Niccolò Mantegna[2], Andrea Maria Zanchettin[2], Paolo Rocco[2]

***Abstract*— This paper tackles the complex task of routing elastic deformable linear objects (DLOs) characterized by considerable stiffness, such as cables or hoses, which are already constrained at both ends. Specifically, a single arm robot is controlled to slide along the unknown contour of the cable, performing collision-free contour following, and to insert specific DLO segments into intermediate known clips. The contour following motion is executed avoiding both collisions with static obstacles and excessive deformation of the manipulated DLO. In particular, the path is defined considering an artificial potential field that is updated after each sliding motion along the DLO. This field accounts for static obstacles, the local cable shape (reconstructed using tactile sensors on the gripper fingertips) and the estimation of the global DLO shape obtained from a dynamic model of the DLO, accounting for the constraints imposed by the clips and the gripper. The proposed method is experimentally validated on an industrial robot executing cable routing in several DLO configurations.**

I. Introduction

In the assembly of various electromechanical systems, such as vehicles, aircraft, and white goods, the operations involving Deformable Linear Objects (DLOs) primarily encompass two tasks: cable routing and cable fixation [1]. The automation of these tasks is challenging due to the complexities involved in the robotic manipulation of DLOs: several problems must be addressed [2]. This work focuses on cable routing tasks, aiming at developing a method for routing an elastic DLO with significant stiffness fixed at both ends. The DLO must be inserted into intermediate clips of known poses, as depicted in Figure 1. The objective is to prevent both excessive deformation of the manipulated DLO and collisions with known static obstacles in the workspace during the motion. Thanks to the proposed method, a single-arm robot can reliably perform cable routing by sliding along the cable's unknown contour in the 3D space. Note that, despite the DLO being elastic, it is characterized by a significant stiffness, meaning that its elongation during the routing can be neglected. Thus, the distance travelled by the robot during contour following can be utilized to identify the DLO segments to be clipped into intermediate known clips. In order to define the path to execute collision-free contour following, we introduce an artificial potential field that is updated after every sliding motion along the DLO. The potential field accounts for the presence of static obstacles (including clips), the local cable shape, reconstructed exploiting tactile sensors on the gripper fingertips as done in [3], and the estimation of the global DLO shape obtained by exploiting a dynamical model of the DLO and considering constraints imposed by clips and the gripper.

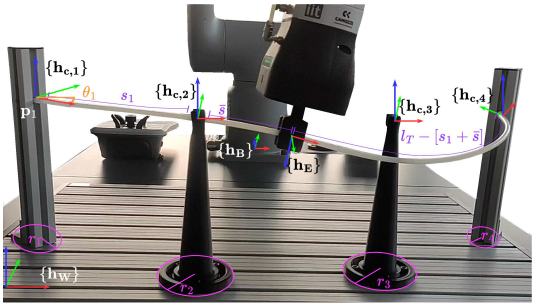

Fig. 1: Robust cable routing with collision avoidance. The DLO is initially constrained in clips $1, 4$ and has to be routed in the intermediate clips $2, 3$. Parameters linked to clip 1 and relevant frames are highlighted. x, y, z axes are depicted in red, green and blue, respectively.

The rest of this work is organised as follows. Section II reviews the related works, emphasizing the contributions of this paper. Section III formalizes the considered problem, while Section IV defines the method to reconstruct the global DLO shape during routing. The definition of the path for collision-free contour following relying on the potential field is detailed in Section V. Finally, Section VI discusses the experimental validation, and Section VII concludes the paper.

II. Related works and contributions

As cable routing is one of the most common assembly operations involving DLOs, several methods addressing this task exist. These strategies can be classified based on the manipulated DLO's stiffness (high or low), the type of sensors used for DLO shape reconstruction (local or global), the initial configuration of the DLO (with one, none, or both ends constrained), and the number of robotic arms involved. Additionally, it is crucial to assess whether the routing strategy includes collision avoidance and contour following skills. Table I summarises the main methodologies and highlights differences from our approach.

[4] presents a strategy exploiting optoelectronic tactile sensors [15] to route an electric wire, following a predefined path and ensuring proper tensioning. Similarly, [5] proposes a planner that concatenates motion primitives to perform cable routing of DLOs with low stiffness based on the local shape reconstructed exploiting Gelsight [16], an optical tactile sensor. Authors of [6] define a vision-based method to perform routing operations of DLOs with low stiffness around pegs. Vision is also exploited in [7], proposing a hierarchical framework where a high-level primitive selection policy chooses the most suitable sequence of

[1]The Author is with Leonardo, Innovation Labs, Robotics, Via Raffaele Pieragostini 80, 16151, Genoa (Italy). e-mail: andrea.monguzzi@leonardo.com
[2]The Authors are with Politecnico di Milano, Dipartimento di Elettronica, Informazione e Bioingegneria, Piazza Leonardo da Vinci 32, 20133, Milan (Italy). e-mail: niccolo.mantegna@mail.polimi.it, {andreamaria.zanchettin, paolo.rocco}@polimi.it

Paper	DLO Stiffness	Shape Est.	External Sensors	Collision Considered	Constrained ends	Arms	Contour following
[4, 5]	Low	Local	Tactile	No	1	1	Yes
[6]	Low	Local	Vision	No	0	2	No
[7]	Low	Local	Vision	No	1	1	No
[8]	Low	Local	\	No	1	2	Yes
[9]	Low	Global	Vision	No	1	2	No
[10]	Low	Global	Force	No	0	2	Yes
[11]	Low	Global	Vision	Yes	0	2	No
[12]	Low	Global	Force, Vision	Yes	0	2	No
[13]	High	Local	Force, Vision, Laser	No	0	3	No
[14]	High	Local	Vision	No	1	1	No
[3]	High	Local	Tactile	No	2	1	Yes
Our	High	Global	Tactile	Yes	2	1	Yes

TABLE I: Summary of the comparison of our strategy with the most relevant existing methods to realize cable routing ("Shape Est." denotes if the DLO shape estimated is local or global, while "Constrained ends" defines the number of constrained DLO ends. "Arms" indicates the numbers of robotic arms used to manipulated the DLO).

learned or scripted primitives to complete the routing. [8] defines a sensorless cable tracing skill enabling a robotic arm to track the unknown contour of a cable held for a small portion by a fixture, and to detect its ends that can be routed. The DLO local shape is geometrically estimated by interpolating the past positions of the tool center point (TCP). The method defined in [9] plans a sequence of learned primitives to route a rope-like DLO by considering spatial relations between the DLO and the environment, exploiting vision to define the global DLO shape. [10] uses instead data obtained from a force sensor to route a DLO with low stiffness, maintaining it under tension and updating a linear graph model representing the global DLO shape. Even [11] and [12] address the routing of a DLO with low stiffness estimating its global shape, but they also propose methods to avoid collision with the environment. Specifically, [11] proposes a task planner to define a sequence of primitives based on heuristic rules, checking if the execution of an action could result in a collision or be out of reach and executing a replanning in these cases. [12] details skills to clip the grasped DLO by controlling robots based on contact detection, and to route the DLO by selecting TCP poses that avoid collisions between the two used robotic arms and the fixtures.

The routing of stiff DLOs is instead addressed in [3, 13, 14]. In [13], several sensors and three robotic arms are exploited to perform the routing of a wire harness performing actions such as clip, twist and regrasp, while [14] details a strategy to insert a DLO into channel clips executing skills as grasp, insert, push and slide. [3] highlights the challenges associated with routing stiff DLOs constrained at both ends and addresses this issue by proposing a set of skills guided by the data acquired from capacitive tactile sensors [17]. Specifically, the robot performs contour following relying on the estimated local shape of the DLO, assuming that the DLO configuration during routing remains distant from the clips so that collisions cannot happen.

The artificial potential field formalism [18] has been broadly used in robotics, however, few works exploit it in manipulating DLO. [19] proposes a teleoperation framework to manipulate DLOs: an attractive potential field toward the reconstructed DLO shape is exploited for precise grasp of the cable, forcing the teleoperated robotic arm to move over the DLO. [20] and [21] exploit potential fields to deal with shape control problems where the goal is to move the DLO in a desired shape. In [21], the robotic arm, grasping the end of the cable, is controlled to insert it in a socket while bending the DLO to avoid collision with the environment. Finally, [1] proposes a method to replan the path of the TCPs of a dual-arm robot manipulating a DLO from an initial shape to a final one in case of collisions of the DLO with obstacles by defining an artificial potential field.

With respect to previous works, the main contributions of our methodology can be identified as follows:

- We propose a potential field-based method for robust cable routing of elastic cables with significant stiffness constrained at both ends avoiding collisions with obstacles and excessive deformation of the DLO. As shown in Table I, the collision-free routing of DLOs with considerable stiffness has not been dealt with in the literature. Unlike [11] and [12], we do not use vision sensors to determine a collision-free path. Additionally, our strategy differs from [20, 21] as we do not use the potential field for shape control problems, and from [1] as we generate a new potential field after each movement, rather than only in the case of collision risk.
- In our method, DLO contour following is guided by a potential field incorporating obstacles positions, the locally reconstructed DLO shape using tactile sensors, and an estimated global DLO shape that considers both geometrical and physical aspects, relying on a dynamical mass-spring model of the DLO [22]. As shown in Table I, the only other work considering the DLO global shape when performing contour following is [10], which exploits a path graph to define the global DLO shape geometrically. However, the path graph is only suitable for low-stiffness DLOs under tension, while this work addresses the routing of stiff DLOs, where bending strain must be considered and tension must be avoided.

III. Problem Formalization

The routing problem is formalized by defining the list $\mathbf{C} = \{\mathbf{c}_1, \ldots, \mathbf{c}_N\}$. Each element $\mathbf{c}_i$, $i = 1, \ldots, N$ contains information of a clip where the DLO has to be routed. In the initial configuration, the DLO is inserted in the first ($\mathbf{c}_1$) and last clip ($\mathbf{c}_N$), having hence both ends constrained. We denote with $\{\mathbf{h}_B\}$ the robot base frame, with $\{\mathbf{h}_E\}$ the end effector one centred in the TCP, with $\{\mathbf{h}_{c,i}\}$ the

frame of clip $\mathbf{c}_i$, and with $\{\mathbf{h}_W\}$ the world frame (Figure 1). The pose of $\{\mathbf{h}_E\}$ is defined by the position of its origin $\mathbf{p}_E = [x_E, y_E, z_E]^\top$ and the quaternion $\mathbf{Q}_E$. These quantity are grouped in $\mathbf{G}_E = \{\mathbf{p}_E, \mathbf{Q}_E\}$. Each clip is described by the known tuple $\mathbf{c}_i = [\mathbf{p}_i, \theta_i, s_i, r_i]$ where:

- $\mathbf{p}_i = [x_i, y_i, z_i]^\top$ is the position where the DLO has to be clipped.
- θ_i is the rotation of the x-axis of $\{\mathbf{h}_{ci}\}$ with respect to the one of $\{\mathbf{h}_W\}$ (it is assumed that the clipped segments of DLO are parallel to the xy plane of $\{\mathbf{h}_W\}$).
- s_i is the distance measured along the routed DLO profile from $\mathbf{p}_i$ to $\mathbf{p}_{i+1}$, identifying the portion of DLO that must be clipped in $\mathbf{c}_i$ (s_N is not defined).
- r_i is the radius of the minimum cylinder that includes the clip and whose axis is aligned with the principal direction of the structure of the clip.

The robot has to route the DLO in all the intermediate clips ($i = 2, \dots, N-1$), performing contour following while avoiding both collisions with obstacles (as clips) and excessive deformation of the DLO, preventing cable damage or cable exit from clips where it has been inserted previously. Each time a segment of DLO is inserted in the corresponding clip $\mathbf{c}_i$, $\mathbf{c}_i$ is added to the list $\bar{\mathbf{C}}$, grouping the clips in which the DLO has been already inserted, and sorting the elements in ascending order based on their index. The considered DLO initial configuration is characterized by $\bar{\mathbf{C}} = \{\mathbf{c}_1, \mathbf{c}_N\}$. $\bar{s}$ denotes the length computed during the contour following along the DLO between the robot TCP and the last clip where the DLO has been inserted. A schematic representation of the mentioned quantities is shown in Figure 1.

Other static obstacles $\boldsymbol{\omega}_\kappa$, $\kappa = N+1, \dots, M$ are grouped in the set $\boldsymbol{\Omega} = \{\boldsymbol{\omega}_{N+1}, \dots, \boldsymbol{\omega}_M\}$. Each $\boldsymbol{\omega}_\kappa$ is described by r_κ and $\mathbf{p}_\kappa$, where r_κ is the radius of the minimum cylinder including the obstacle and $\mathbf{p}_\kappa$ indicates the point on the axis of the cylinder with the highest z coordinate.

The robotic arm is equipped with a parallel gripper allowing the position control of the fingers opening and closing. The gripper features two sensorized fingers described in [17]. Specifically, each finger is equipped with a capacitive tactile sensor, formed by a 5×4 matrix of taxels (see Figure 2a), able to sense the normal deformation (for more details refer to [3, 17]). As explained in [3], once the DLO is positioned between the fingers, it is possible to close the gripper on it allowing both to sense its local shape and slide along its contour. [3] describes a method to reconstruct the local shape of the DLO and predict its local future shape (i.e. the shape in the DLO portion in close proximity to the grasped one). In particular, [3] details the computation of the parameters α, q describing the grasped DLO planar shape, and γ indicating the local curvature (Figure 2b,c).

IV. Global Shape Estimation of a Routed DLO

To estimate the global shape of the elastic DLO during routing, we resort to the mass-spring dynamic model presented in [22]. As shown in Figure 3, a DLO of mass m_T and length l_T is modelled as a sequence of n cable links of length l_j, $j = 1, \dots, n$, and $n+1$ equally spaced mass-points having

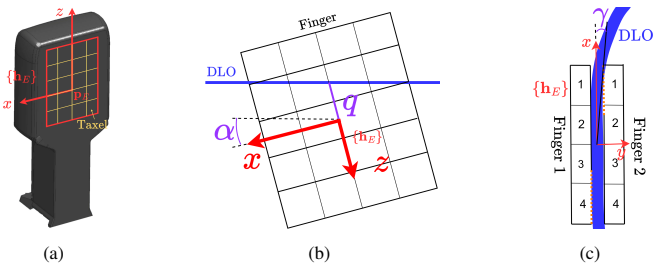

(a) (b) (c)

Fig. 2: (a) Structure of the capacitive tactile sensor mounted on each finger. Parameters α and q describing the grasped DLO planar shape (b) and γ related to the local curvature (c) are defined according to [3].

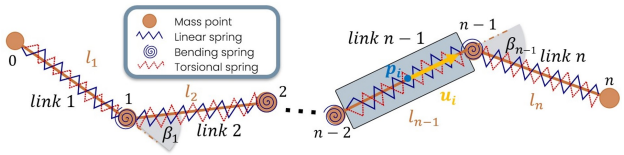

Fig. 3: Mass-spring model of the DLO [22]. Angles β_j are necessary to compute $\mathbf{F}_j^B$. Link $n-1$ is clipped by clip $\mathbf{c}_i$ (the unit vector $\mathbf{u}_i$ is highlighted).

mass $m_j = m_T/(n+1)$, $j = 0, \dots, n$, connected by three different types of springs, describing stretching, bending and torsional strains. In this work, we assume that the fully routed configuration does not involve torsion, and we neglect the torsional strain since the DLO ends are already constrained. The state of the model at time t is given by $\boldsymbol{\epsilon}_j(t)$ $j = 0 \dots n$, where $\boldsymbol{\epsilon}_j(t) = [x_j(t), y_j(t), z_j(t)]^\top$ contains the position of the j - th mass-point. The equation of motion of each mass-point is obtained by exploiting Newton's second law:

$$m_j \ddot{\boldsymbol{\epsilon}}_j(t) = -k^d \dot{\boldsymbol{\epsilon}}_j(t) + \mathbf{F}_j^S(t) + \mathbf{F}_j^B(t) + \mathbf{F}_j^E(t) \quad (1)$$

where $\mathbf{F}_j^S$ and $\mathbf{F}_j^B$ are the elastic force and the bending one, respectively (see [22, 23] for the detailed computation) and $\mathbf{F}_j^E$ collects the external forces, also accounting for the gravity effect. k^d is a fictitious damping coefficient introduced to mitigate oscillatory behaviours. Given the initial cable configuration, $\mathbf{F}_j^S$ and $\mathbf{F}_j^B$ can be computed. Equation (1) can then be explicitly integrated by exploiting Euler Method to obtain the acceleration $\mathbf{a}_j(t)$, the velocity $\mathbf{v}_j(t)$ and, finally, the position $\boldsymbol{\epsilon}_j(t)$ of mass point j.

To model the DLO shape during routing, the interaction with static clips and the robot gripper is considered. Specifically, a static clip/gripper grasping the DLO interacts with one of its links (Figure 3). The position $\mathbf{p}_i$ of a clip grasping link j constrains the position of the mass-points $j-1$ and j: $\boldsymbol{\epsilon}_{j-1}(t) = \mathbf{p}_i - (l_j/2)\mathbf{u}_i$, $\boldsymbol{\epsilon}_j(t) = \mathbf{p}_i + (l_j/2)\mathbf{u}_i$ where $\mathbf{u}_i$ is the direction vector aligned with the x axis of $\{\mathbf{h}_{c,i}\}$ expressing the orientation θ_i, and l_j is the length of the constrained link. Similar arguments hold for the gripper holding the cable after a motion along it. For the mass points $j-1$ and j, we added the external forces to account for the static constraint: $\mathbf{F}_j^E(t) = k^d \mathbf{v}_j(t) - \mathbf{F}_j^S(t) - \mathbf{F}_j^B$ (similar arguments hold for $\mathbf{F^E}_{j-1}(t)$).

As detailed in Section V, the robot executes contour following performing discrete motions: after each movement, the artificial potential field is updated requiring the estimation of the DLO global shape. The described dynamical model

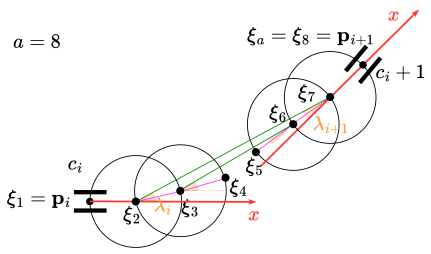

Fig. 4: Definition of λ_i, λ_{i+1} to determine the points $\boldsymbol{\xi}_k$, $k = 1, \ldots, a$ with $a = 8$ used to define the spline $\mathcal{S}_i$ that interpolates $\boldsymbol{\xi}_k$ (top view).

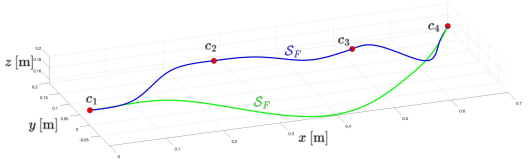

Fig. 5: Estimated global shape $\mathcal{S}_F$ for DLO in the initial configuration (green) and fully routed in four clips (blue).

has to be initialized specifying $\boldsymbol{\epsilon}_j(0)$ $(j = 0, \ldots, n)$ each time an update of the potential field is required. To this aim, we define the strategy summarized in Algorithm 1. It takes as input the DLO total length l_T, the set of clips where the DLO has been already inserted $\bar{\mathbf{C}}$, and the pose of $\{\mathbf{h}_E\}$. A spline $\mathcal{S}_i$ is fitted between consecutive clips or between a clip and the TCP (lines $1-12$). Algorithm 2 summarizes the procedure to define $\mathcal{S}_i$ between $\mathbf{c}_i$ and $\mathbf{c}_{i+1}$, sketched in Figure 4. Similar arguments are used to define the spline between the last clip where the DLO has been inserted and the TCP and between the TCP and $\mathbf{c}_N$. In these last cases, the position of the TCP must be used, and $\bar{s}$ and $l_T - [\bar{s} + \sum_i s_i]$ $\forall \mathbf{c}_i \in (\bar{\mathbf{C}} \setminus \{\mathbf{c}_N\})$ (see Figure 1) have to be used instead of s_i in Algorithm 2, respectively. According to Algorithm 1, a total spline $\mathcal{S}_T$ is defined by joining the computed $\mathcal{S}_i$ and a first definition of the $\boldsymbol{\epsilon}_j(0)$ $(j = 0, \ldots, n)$ is obtained (lines $13-14$). Finally, the positions $\boldsymbol{\epsilon}_j(0)$ are refined by executing a check on the total length of the obtained $\mathcal{S}_T$, scaling it to match l_T (lines $15-20$). Equation (1) is finally used to simulate the grasped and clipped DLO considering the gravity effect. The simulation is executed until all the mass-points reach velocities close to zero a time $\bar{t}$: the obtained $\boldsymbol{\epsilon}_j(\bar{t})$ are used to define a spline $\mathcal{S}_F$ representing the final global shape. To initialize the dynamical model, the values of the following parameters of the DLO are required [22]: total mass m_T, total length l_T, diameter, cross-section area, Young's elastic modulus (that can be estimated as in [24]), and Poisson's ratio. Figure 5 shows examples of estimated global shapes $\mathcal{S}_F$ in different stages of the routing procedure.

V. Artificial Potential Field for Collision-Free Contour Following

The proposed routing procedure, summarized in Figure 6, begins with the robot closing the gripper fingertips on the DLO segment emerging from clip $\mathbf{c}_1$. Utilizing tactile data, we compute the appropriate finger distance D to slide along the DLO without generating excessive friction force between the cable and the sensors while maintaining the DLO between the fingers for proper shape sensing (first left

Algorithm 1: Initialization of the DLO dynamic model after a sliding motion along the cable or a clipping operation

Input: $\bar{\mathbf{C}}$, $\mathbf{G}_E = \{\mathbf{p}_E, \mathbf{Q}_E\}$, l_T
Output: $\boldsymbol{\epsilon}_j(0)$ (with $j = 0, \ldots, n$)
1: $\mathcal{S}_i \leftarrow$ null $(i = 1, \ldots, N)$, $\mathcal{S}_T \leftarrow$ null, $\boldsymbol{\epsilon}_j(0) \leftarrow$ null $(j = 0, \ldots, n)$, $l_S \leftarrow$ null, $i = 1$, $K = 1$
Check if the gripper is manipulating the DLO
2: **if** robot is performing contour following **then**
3: **for** $i = 1 :$ (card$(\bar{\mathbf{C}}) - 2$) **do** {card$(\cdot)$ outputs the cardinality of a set}
4: $\mathcal{S}_i \leftarrow$ spline between $\mathbf{c}_i$ and $\mathbf{c}_{i+1}$
5: **if** card$(\bar{\mathbf{C}}) - 1 \neq 0$ **then**
6: $i \leftarrow i + 1$
7: $\mathcal{S}_i \leftarrow$ spline between $\mathbf{c}_i$ and $\mathbf{G}_E$
8: $i \leftarrow i + 1$
9: $\mathcal{S}_i \leftarrow$ spline between $\mathbf{G}_E$ and $\mathbf{c}_N$
10: **else**
11: **for** $i = 1 :$ (card$(\bar{\mathbf{C}}) - 1$) **do**
12: $\mathcal{S}_i \leftarrow$ spline between $\mathbf{c}_i$ and $\mathbf{c}_{i+1}$
13: $\mathcal{S}_T \leftarrow$ spline joining the computed $\mathcal{S}_i$
Compute rough mass-points positions
14: $\boldsymbol{\epsilon}_j(0) \leftarrow$ interpolation of a set of n equally spaced points along $\mathcal{S}_T$
15: $l_S \leftarrow$ length of $\mathcal{S}_T$
Refine total spline to adjust length
16: **while** $|l_T - l_S| > L$ **do**
17: $K \leftarrow K \cdot l_T / l_S$
18: $\boldsymbol{\epsilon}_j(0) \leftarrow \boldsymbol{\epsilon}_j(0) \cdot K$ (with $j = 0, \ldots, n$)
19: $\mathcal{S}_T \leftarrow$ spline interpolating $\boldsymbol{\epsilon}_j(0)$ (with $j = 0, \ldots, n$)
20: $l_S \leftarrow$ length of $\mathcal{S}_T$

Algorithm 2: Spline definition between $\mathbf{c}_i$ and $\mathbf{c}_{i+1}$

Input: $\mathbf{c}_i$, $\mathbf{c}_{i+1}$, a (even number defining the number of points $\boldsymbol{\xi}_k$ to fit $\mathcal{S}_i$)
Output: $\mathcal{S}_i$
1: $\boldsymbol{\xi}_k \leftarrow$ null$(k = 1, \ldots, a)$, $d = 0$, $\lambda_i = 0$, $\lambda_{i+1} = 0$, $\mathcal{S}_i \leftarrow$ null
2: d $= s_i/(a-1)$
3: $\boldsymbol{\xi}_1 = \mathbf{p}_i$, $\boldsymbol{\xi}_a = \mathbf{p}_{i+1}$
4: Define $\boldsymbol{\xi}_2$ translating $\boldsymbol{\xi}_1$ of d along x of $\{\mathbf{h}_{c,i}\}$
5: Define $\boldsymbol{\xi}_{a-1}$ translating $\boldsymbol{\xi}_a$ of d along $-x$ of $\{\mathbf{h}_{c,i+1}\}$
6: **for** $k = 3 : a/2$ **do**
7: $\lambda_i \leftarrow$ angle between x of $\{\mathbf{h}_{c,i}\}$ and segment joining $\boldsymbol{\xi}_{k-1}, \boldsymbol{\xi}_{a-k+2}$
8: $\lambda_{i+1} \leftarrow$ angle between $-x$ of $\{\mathbf{h}_{c,i+1}\}$ and segment joining $\boldsymbol{\xi}_{k-1}, \boldsymbol{\xi}_{a-k+2}$
9: $\boldsymbol{\xi}_k(1,2) \leftarrow x, y$ coordinates of the point identified by $\lambda_i/2$ on the circumference of radius d and centre $\boldsymbol{\xi}_{k-1}$
10: $\boldsymbol{\xi}_{a-k+1}(1,2) \leftarrow x, y$ coordinates of the point identified by $\lambda_{i+1}/2$ on the circumference of radius d and centre $\boldsymbol{\xi}_{a-k+2}$
11: $\boldsymbol{\xi}_k(3) \leftarrow 0.8 \cdot \boldsymbol{\xi}_{k-1}(3) + 0.2 \cdot \boldsymbol{\xi}_{a-k+2}(3)$
12: $\boldsymbol{\xi}_{a-k+1}(3) \leftarrow 0.2 \cdot \boldsymbol{\xi}_{k-1}(3) + 0.8 \cdot \boldsymbol{\xi}_{a-k+2}(3)$
13: $\mathcal{S}_i \leftarrow$ spline defined using $\boldsymbol{\xi}_k$, $k = 1, \ldots, a$

block in Figure 6). Specifically, the fingertips gradually close until the measurements acquired from the taxels overcome a user-defined threshold. Then, the robot performs a series of discrete motions along the cable profile: after each movement, a new collision-free path is generated to follow the next cable portion relying on the updated artificial potential field. The parameters α, q, γ describing the DLO local shape (Figure 2b,c) are computed as in [3] exploiting tactile data (grey block in Figure 6). The fingertips are then aligned to the local shape of the cable, by compensating first the misalignment expressed by q, then the one by α and finally the one of γ, as explained in [3] (blue block in Figure 6). At this point the x axis of $\{\mathbf{h}_E\}$ is locally aligned with the profile of the cable. The quantity $\Delta\chi$ can be used as an estimation of the length, measured from the TCP, by which the cable will locally assume a straight-line shape aligned with the x axis of $\{\mathbf{h}_E\}$. $\Delta\chi$ is computed as in [3]:

$$\Delta\chi = W_c / \sqrt{W_\alpha \alpha^2 + W_q q^2 + W_\gamma \gamma^2} \qquad (2)$$

where $W_c, W_\alpha, W_q, W_\gamma$ are positive user-defined weights. The global shape of the routed DLO is then estimated as

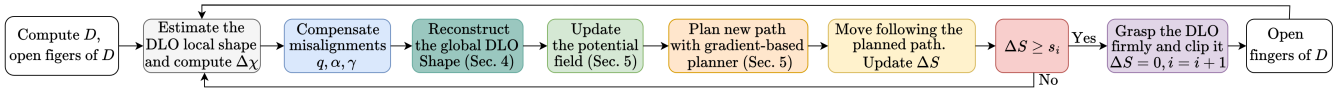

Fig. 6: Flowchart of the proposed iterative procedure to realize robust cable routing.

explained in Section IV (dark green block in Figure 6). This information, together with the estimate of the local shape and the presence of obstacles (including clips) are used to define the artificial potential field $\mathcal{P}$ (light green block in Figure 6), as better detailed in the following. A gradient-based planner is exploited to find a collision-free path for the TCP along $\mathcal{P}$ (orange block in Figure 6), allowing the robot to slide along the cable and reach a DLO portion in the proximity of the one predicted at distance $\Delta\chi$. A variable ΔS is updated adding the distance travelled along the DLO contour (yellow block in Figure 6). Note that when ΔS approaches s_i, the value W_c in (2) is set to a lower value $\bar{W}_c$ to restrain the length travelled at every movement, to reach precisely s_i. This procedure is iterated until $\Delta S \geq s_i$ (red block in Figure 6). At this point, the robot stops the sliding motion and securely grasps the reached cable segment by closing the gripper fingers. It then performs a clipping operation in clip $\mathbf{c}_i$ (purple block in Figure 6). Clipping operation are executed according to scripted skills that move the TCP to an approach position and an insertion one and are not affected by the effect of the potential field. After the insertion, the gripper fingers are then opened by D (last block on the right in Figure 6), and the procedure described above is repeated until the cable is inserted into clip $\mathbf{c}_{N-1}$, completing the routing operation.

As mentioned, after each motion along the cable profile and clipping operation, an artificial potential field $\mathcal{P}$ is updated. $\mathcal{P}$ is exploited to establish a path for the robot TCP to slide along a DLO portion while preventing both the gripper from approaching obstacles too closely (to avoid collisions) and excessive deformation of the DLO shape. Specifically, $\mathcal{P}$ is defined by the combination of an attractive field $\mathcal{A}$ and a repulsive field $\mathcal{R}$.

The attractive field $\mathcal{A}$ is designed as a Gaussian potential field. Its unique stationary point $\mathbf{O}_T = [x_{OT}, y_{OT}, z_{OT}]$ is computed considering the points $\mathbf{O}_L$ and $\mathbf{O}_G$. The former defines the future local shape estimation corresponding to $\Delta\chi$, while the latter is the point on the global estimated shape $\mathcal{S}_F$ evaluated at the same x coordinate of $\mathbf{O}_L$. Specifically, after a planned movement or clipping operation at time $\tilde{t}$, $\mathbf{O}_L(\tilde{t}) = [x_E(\tilde{t}) + \Delta\chi(\tilde{t}),\ y_E(\tilde{t}),\ z_E(\tilde{t})]^\top$, while $\mathbf{O}_G(\tilde{t}) = [x_E(\tilde{t}) + \Delta\chi(\tilde{t}),\ y_{OG},\ z_{OG}]$, where y_{OG}, z_{OG} are the y and z coordinates obtained evaluating $\mathcal{S}_F$ (computed at $\tilde{t}$) in $x_E(\tilde{t}) + \Delta\chi(\tilde{t})$. We hence define $\mathbf{O}_T(\tilde{t}) = (W_L\mathbf{O}_L(\tilde{t}) + W_G\mathbf{O}_G(\tilde{t}))/(W_L + W_G)$ where W_L, W_G are positive user-defined weights. $\mathcal{A}$ at time $\tilde{t}$ is computed as (time indices are omitted for sake of readability):

$$\mathcal{A} = z_E + (z_{OT} - z_E) \cdot exp\left(-\frac{(x - x_{OT})^2 + (y - y_{OT})^2}{2\sigma^2}\right) \quad (3)$$

where σ equal to the Euclidean distance from $\mathbf{O}_T$ to the current grasping position $\mathbf{p}_E$. To avoid situations of nearly zero gradient on $\mathcal{A}$, if $|z_{OT}(\tilde{t}) - z_E(\tilde{t})| < \mu$ then $z_{OT}(\tilde{t}) = z_{OT}(\tilde{t}) + \mu$, where μ is a user designed threshold. According to equation (3), $\mathcal{A}$ has a minimum in $\mathbf{O}_T$ if $z_{OT} - z_E < 0$, or a maximum at $\mathbf{O}_T$ if $z_{OT} - z_E > 0$. Based on whether $\mathcal{A}$ exhibits a minimum or a maximum, the gradient-based planner for the TCP path will proceed along the descending or ascending direction of the gradient along the potential filed $\mathcal{P}$, as detailed in the following.

To define the repulsive field $\mathcal{R}$, a field $\mathcal{R}_h$, with $h = 1, \ldots, N, N+1, \ldots, M$ is computed for each clip $\mathbf{c}_i \in \mathbf{C}$ and $\boldsymbol{\omega}_\kappa \in \boldsymbol{\Omega}$. In particular, each $\mathcal{R}_h$ is defined by the combination of two repulsive fields $\mathcal{R}_h^1$ and $\mathcal{R}_h^2$. $\mathcal{R}_h^1$ is a cylindrical field with height equal to the z coordinate of $\mathbf{p}_h$, and radius r_h. $\mathcal{R}_h^2$ is a hemispherical field of radius r_h and is defined on top of $\mathcal{R}_h^1$. In the following, generic points belonging to $\mathcal{R}_h^1$ and $\mathcal{R}_h^2$ are denotes as $\boldsymbol{\rho}_h^{R1} = [x_h^{R1}, y_h^{R1}, z_h^{R1}]$ and $\boldsymbol{\rho}_h^{R2} = [x_h^{R2}, y_h^{R2}, z_h^{R2}]$, respectively. Depending on z_E, $\mathcal{R}_h$ linked to the object (clip or obstacle) h is defined according to the following rules:

A) $z_e \leq \mathbf{p}_h \rightarrow \mathcal{R}_h = \{\boldsymbol{\rho}_h^{R1} \in \mathcal{R}_h^1 \mid z_h^{R1} \geq z_e,\ \forall\, \boldsymbol{\rho}_h^{R2} \in \mathcal{R}_h^2\}$

B) $\mathbf{p}_h < z_e \leq (\mathbf{p}_h + r_h) \rightarrow \mathcal{R}_h = \{\boldsymbol{\rho}_h^{R2} \in \mathcal{R}_h^2 \mid z_h^{R2} \geq z_e\}$

C) $\mathbf{p}_h > (\mathbf{p}_h + r_h) \rightarrow \mathcal{R}_h = \{\}$

A smooth connection between $\mathcal{R}_h$ and the horizontal reference plane where the TCP position $\mathbf{p}_E$ lays is achieved by defining a *falloff* distance $d_h > r_h$ [25] beyond which the repulsion effect becomes negligible. If two or more $\mathcal{R}_h$ overlaps and $\mathbf{p}_E$ is close to their repulsive regions, the shape of the repulsive fields overlapping is modified by making their horizontal section elliptical [26], as shown in Figure 7. In particular, the elliptical sections have a major axis $\Gamma_{1h} = 2r_h$, and a minor axis Γ_{2h} whose magnitude depends on the Euclidean distance between $\mathbf{p}_E$ and $\mathbf{p}_h$: $\Gamma_{2h} = 2r_h^2/||\mathbf{p}_E - \mathbf{p}_h||_2$. It is enforced $\Gamma_{2h} > \Gamma_{min}$ to prevent collisions. As shown in Figure 7, Γ_{1h} aligns with the direction between the current grasping point and the stationary point $\mathbf{O}_T$ of $\mathcal{A}$ (defined by angle ϕ), creating a valley in the portion of space where the DLO locally lays, allowing contour following with collision avoidance also between close obstacles. Finally, if $z_{OT} > z_E$ ($\mathcal{A}$ exhibits a maximum) the gradient-based path planner has to follow an increasing direction of the gradient searching for the maximum: it follows that, to allow a proper definition of the path of the TCP, the portions of $\mathcal{R}_h$ having points with $z_h^R > z_E$ must be mirrored with respect to a plane including $\mathbf{p}_E$ and parallel to the xy plane of $\{\mathbf{h}_W\}$, creating M minima. Examples of the total potential field $\mathcal{P}$ for $z_E > z_{OT}$ and $z_E < z_{OT}$ are shown in Figure 8.

Once the artificial potential field $\mathcal{P}$ is defined, a gradient-based planner is applied to define a path from the TCP current pose to the stationary point $\mathbf{O}_T$ of $\mathcal{A}$, following with

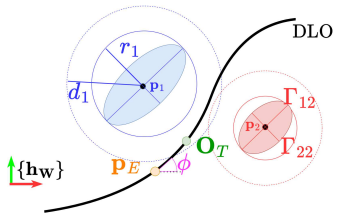

Fig. 7: Example of the reshaping of the repulsive fields of two obstacles $h = 1, 2$ (top view). The *falloff* distance d_h, the radius r_h, the ellipse axes Γ_{1h}, Γ_{2h} and the angle ϕ are highlighted.

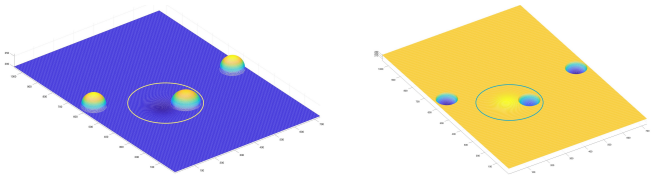

(a) (b)

Fig. 8: Definition of $\mathcal{P}$ for (a) $z_E > z_{OT}$, (b) $z_E < z_{OT}$.

a fixed step size the descending direction of the gradient if $z_E > z_{OT}$ or the ascending one if $z_E < z_{OT}$, stopping according to a user-defined tolerance. The obtained path is fitted with a cubic polynomial function to ensure smoothness and a good approximation of the real DLO local shape. The TCP orientation at the final point $\mathbf{O}_T$ of the path is computed as a linear spherical interpolation (Slerp) of the quaternions $\mathbf{Q}_E$ and $\mathbf{Q}_G$: the first describes the actual orientation of the TCP frame $\{\mathbf{h}_E\}$ (aligned with the local estimated cable shape) while the second one is the orientation of a frame with the x axis tangent in $\mathbf{O}_G$ to the global estimated shape $\mathcal{S}_F$ and oriented in the direction of motion, with the y axis on the same side of the DLO as the one of $\{\mathbf{h}_E\}$. The maximum velocity for each motion is set to a user-defined value.

VI. Experimental Validation

The robot used in the experimental validation is a GoFa by ABB, equipped with the Smart Gripper manufactured by Camozzi. As DLO it is considered a PA12 hose, characterized by $l_T = 73$ cm, $m_T = 18$ g and a Young modulus of 10^9 Pa. Three different configurations of clips and obstacles are considered as shown in Figure 9. These configurations have been selected so that collision avoidance during contour following is necessary: the strategy proposed in [3] has been applied and collisions between the end effector and the clips/obstacles were observed. Different experiments exploiting the proposed methodology are then executed for each configuration, modifying parameters linked to the dimension of the repulsive regions and to the definition of the stationary point of $\mathcal{A}$, as detailed in the following. The fixed values of the parameters are $n = 19$, $L = 0.5$ cm, $a = 8$, and $\mu = 0.5$ cm. According to [3] the parameters linked to the local shape estimation are set as $W_c = 8$ cm, $\bar{W}_c = 2$ cm $W_\alpha = 0.4$ deg^{-1}, $W_q = 0.02$ cm^{-1}, $W_\gamma = 0.8$deg^{-1}. The tolerance and the step for the gradient-based planner are set to 0.4 cm. The maximum velocity is set to 150 mm/s. The motion of the robot along the computed online paths is executed using linear movements discretizing the paths in intermediate goal poses. The accompanying video[1] shows some of the performed experiments.

Configuration **(I)** (Figure 9a) is selected to analyse the effect of the repulsion field in a case where the DLO passes close to a clip and enters its repulsive zone with a direction almost perpendicular to the circular section of $\mathcal{R}$. A sensitivity analysis is performed by modifying the amplitude of the repulsive region using five different values ranging from 5 cm to 9 cm. The weights for the computation of $\mathbf{O}_T$ are $W_L = 0.5$ and $W_G = 0.5$. As the computed and executed paths reported in Figure 9b shows, the methodology allows to perform contour following avoiding collision also in case the DLO shape enters the repulsive region, leading to a success rate of $5/5$. Configuration **(II)** (Figure 9c) presents two intermediate clips and the DLO shape lying close to them, especially to the second one after the first clipping operation. The effect of the repulsion region has a radius of 5 cm, and a sensitivity analysis is carried out on the values of W_L and W_G. Considering the results shown in Figure 9d, it can be seen that relying solely on either the locally or globally estimated shape results in motion where the DLO is dragged laterally or brought over the clip, respectively. Considering both the global shapes and the locally estimated one leads to preferable intermediate configurations, where the DLO deformation is minor. Two routing experiments are executed for each pair of considered values of W_L and W_G for a total of ten tests: only one routing failed when $W_L = 1, W_G = 0$ since the cable was dragged laterally and its curvature was not properly sensed. Configuration **(III)** (Figure 9e) entails an intermediate clip and two obstacles, whose repulsive fields overlap. The experiments executed in this configuration consider $W_L = 0.5$ and $W_G = 0.5$. As Figure 9f shows, a reshaping of the overlapping fields is executed considering five different values for Γ_{min}, constraining the minimum length of the minor axis of the elliptic section. The reshaping is essential to perform the routing operation successfully: if no reshaping is applied, the robot gets stuck as shown in the green path in Figure 9f. Two routing experiments are executed for each value of Γ_{min} for a total of ten tests: only the ones where reshaping was not applied failed.

VII. Conclusions

This work proposes a potential field-based approach for the online computation of a path to obtain collision-free cable contour following of an elastic DLO with significant stiffness constrained at both ends. This strategy is exploited to perform cable routing avoiding both collision with obstacles and excessive deformation of the DLO. The methodology relies on an attractive field updated by considering the local DLO future shape, estimated by exploiting tactile data, and the DLO global shape, computed relying on a dynamical DLO model and including the constraints exerted by the clips on the DLO. The method was successfully tested in real-world experiments in different DLO configurations. Future work will use vortex artificial potential fields to define repulsive

[1] https://youtu.be/7vKTM3CVP_8

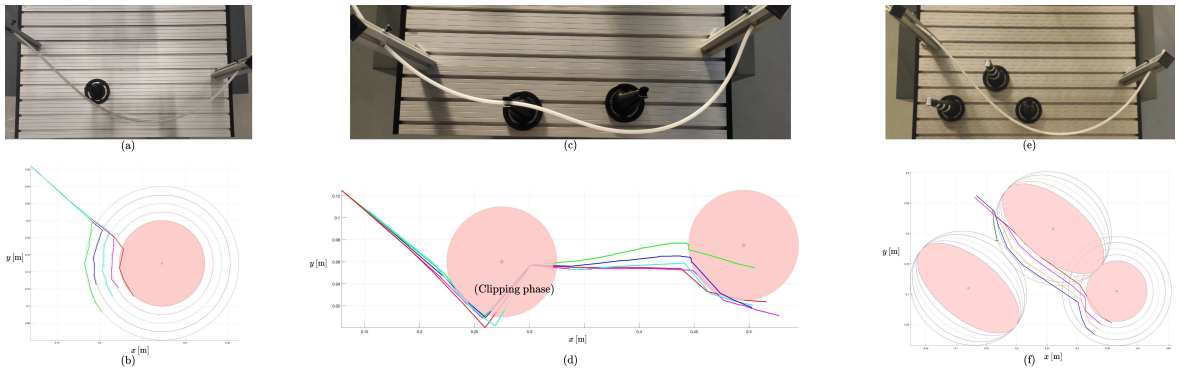

Fig. 9: Configurations considered (top row) and obtained paths during different experiments (bottom row). Note that paths enter the repulsive regions during the clipping phases, when the effect of the potential field is not considered. If a path overlaps the repulsive region during contour following, it indicates that the robot TCP is above the region. (a) Configuration **(I)**. (b) Paths comparison for different amplitudes of repulsive region, from 9 cm (green path), to 5 cm (red path). (c) Configuration **(II)**. (d) Paths comparison for different W_L and W_G: $W_L = 1$, $W_G = 0$ (red), $W_L = 0.7$, $W_G = 0.3$ (pink), $W_L = 0.5$, $W_G = 0.5$ (cyan), $W_L = 0.3$, $W_G = 0.7$ (blue), $W_L = 0$, $W_G = 1$ (green). (e) Configuration **(III)**. (f) Paths comparison for different values of Γ_{min}, ranging from 10 cm (green path), to 5 cm (red path).

fields. Vision data will also be used to reconstruct the DLO shape and included in the definition of the attractive field.

VIII. Acknowledgment

The authors acknowledge Camozzi SpA for providing the gripper and supporting this project. This work was supported by Progetto Prin 2020 "Co-Mir", prot. 2020CMEFPK. The research presented herein was carried out while the author Andrea Monguzzi was enrolled at Politecnico di Milano.

References

[1] J. Guo, J. Zhang, D. Wu, Y. Gai, and K. Chen. "A local manipulation path replanning algorithm on deformable linear objects for collisions resulted from model deviation". In: *Journal of Manufacturing Systems* 65 (2022), pp. 362–377.

[2] J. Zhu, A. Cherubini, C. Dune, D. Navarro-Alarcon, F. Alambeigi, D. Berenson, F. Ficuciello, K. Harada, J. Kober, X. Li, et al. "Challenges and outlook in robotic manipulation of deformable objects". In: *IEEE Robotics & Automation Magazine* 29.3 (2022), pp. 67–77.

[3] A. Monguzzi, M. Pelosi, A. M. Zanchettin, and P. Rocco. "Tactile based robotic skills for cable routing operations". In: *2023 IEEE International Conference on Robotics and Automation (ICRA)*. IEEE. 2023, pp. 3793–3799.

[4] K. Galassi and G. Palli. "Robotic wires manipulation for switchgear cabling and wiring harness manufacturing". In: *2021 4th IEEE International Conference on Industrial Cyber-Physical Systems (ICPS)*. IEEE. 2021, pp. 531–536.

[5] A. Wilson, H. Jiang, W. Lian, and W. Yuan. "Cable Routing and Assembly using Tactile-driven Motion Primitives". In: *2023 IEEE International Conference on Robotics and Automation (ICRA)*. 2023, pp. 10408–10414.

[6] J. Zhu, B. Navarro, R. Passama, P. Fraisse, A. Crosnier, and A. Cherubini. "Robotic manipulation planning for shaping deformable linear objects withenvironmental contacts". In: *IEEE Robotics and Automation Letters* 5.1 (2019), pp. 16–23.

[7] J. Luo, C. Xu, X. Geng, G. Feng, K. Fang, L. Tan, S. Schaal, and S. Levine. "Multi-stage cable routing through hierarchical imitation learning". In: *IEEE Transactions on Robotics* (2024).

[8] A. Monguzzi, A. M. Zanchettin, and P. Rocco. "Sensorless robotized cable contour following and connector detection". In: *Mechatronics* 97 (2024), p. 103096.

[9] S. Jin, W. Lian, C. Wang, M. Tomizuka, and S. Schaal. "Robotic cable routing with spatial representation". In: *IEEE Robotics and Automation Letters* 7.2 (2022), pp. 5687–5694.

[10] F. Süberkrüb, R. Laezza, and Y. Karayiannidis. "Feel the tension: Manipulation of deformable linear objects in environments with fixtures using force information". In: *2022 IEEE/RSJ Intern. Conf. on Intelligent Robots and Systems*. IEEE. 2022, pp. 11216–11222.

[11] G. A. Waltersson, R. Laezza, and Y. Karayiannidis. "Planning and control for cable-routing with dual-arm robot". In: *2022 International Conf. on Robotics and Automation*. IEEE. 2022, pp. 1046–1052.

[12] K. Chen, Z. Bing, F. Wu, Y. Meng, A. Kraft, S. Haddadin, and A. Knoll. "Contact-aware Shaping and Maintenance of Deformable Linear Objects With Fixtures". In: *2023 IEEE/RSJ International Conference on Intelligent Robots and Systems (IROS 2023)*. 2023.

[13] X. Jiang, K.-m. Koo, K. Kikuchi, A. Konno, and M. Uchiyama. "Robotized assembly of a wire harness in a car production line". In: *Advanced Robotics* 25.3-4 (2011), pp. 473–489.

[14] P. Chang, R. Luo, M. Zolotas, and T. Padır. "Manipulation of Deformable Linear Objects in Benchmark Task Spaces". In: *2022 IEEE 18th International Conference on Automation Science and Engineering (CASE)*. IEEE. 2022, pp. 1910–1916.

[15] A. Cirillo, G. De Maria, C. Natale, and S. Pirozzi. "Design and evaluation of tactile sensors for the estimation of grasped wire shape". In: *2017 IEEE International Conference on Advanced Intelligent Mechatronics (AIM)*. IEEE. 2017, pp. 490–496.

[16] W. Yuan, S. Dong, and E. H. Adelson. "Gelsight: High-resolution robot tactile sensors for estimating geometry and force". In: *Sensors* 17.12 (2017), p. 2762.

[17] R. A. Romeo, A. Zocco, A. Parmiggiani, A. Mura, M. Gesino, M. Accame, M. Maggiali, and L. Fiorio. "Instrumenting a Robotic Finger to Augment the Capabilities of Robotic Grippers". In: *IEEE Trans. on Instrumentation and Measurement* 72 (2023), pp. 1–11.

[18] O. Khatib. "Real-time obstacle avoidance for manipulators and mobile robots". In: *The international journal of robotics research* 5.1 (1986), pp. 90–98.

[19] D. Chiaravalli, A. Caporali, A. Friz, R. Meattini, and G. Palli. "A Vision-based Shared Autonomy Framework for Deformable Linear Objects Manipulation". In: *2023 IEEE/ASME Intern. Conf. on Advanced Intelligent Mechatronics*. IEEE. 2023, pp. 733–738.

[20] X. Li, Z. Wang, and Y.-H. Liu. "Sequential robotic manipulation for active shape control of deformable linear objects". In: *2019 IEEE International Conference on Real-time Computing and Robotics (RCAR)*. IEEE. 2019, pp. 840–845.

[21] C. Jiao, X. Jiang, X. Li, and Y. Liu. "Vision based cable assembly in constrained environment". In: *2018 IEEE International Conference on Robotics and Biomimetics (ROBIO)*. IEEE. 2018, pp. 8–13.

[22] N. Lv, J. Liu, X. Ding, J. Liu, H. Lin, and J. Ma. "Physically based real-time interactive assembly simulation of cable harness". In: *Journal of Manufacturing Systems* 43 (2017), pp. 385–399.

[23] L. Fattorelli. "Dynamic model of a deformable linear object with environmental interactions for robotic manipulation". In: *Politesi, Master thesis*. 2021.

[24] G. Palli and S. Pirozzi. "Validating DLO Models from Shape Observation". In: *2021 IEEE/ASME International Conference on Advanced Intelligent Mechatronics (AIM)*. IEEE. 2021, pp. 430–435.

[25] G. Bell and M. Weir. "Forward chaining for robot and agent navigation using potential fields". In: *Proceedings of the 27th Australasian conference on Computer science-Volume 26*. 2004, pp. 265–274.

[26] H. Yufeng, L. Xiang, L. Long, D. Yingchang, and Z. Xingjing. "Online Path Planning of Mobile Robots Based On Elliptic Influence Domain and Improved Artificial Potential Field". In: *2019 IEEE 4th Advanced Information Technology, Electronic and Automation Control Conference (IAEAC)*. IEEE. 2019, pp. 938–943.